Volume 21, No 2 | International Journal of Radiation Research, April 2023

Investigating geometric and dosimetric accuracy of auto-segmentation contours in stereotactic body radiation therapy for early peripheral non-small cell lung cancer

Z. Chen[1*], X. Lv[2#], Y. Bai[1], L. Xu[1], W. Shao[3*]

[1]*Department of Radiation Therapy, the First Affiliated Hospital of Harbin Medical University, Harbin, Heilongjiang 150001, China*

[2]*Department of Radiation Oncology, the First Affiliated Hospital of Jiamusi University, Jiamusi, Heilongjiang 154003, China*

[3]*Department of Radiation Physics, Harbin Medical University Cancer Hospital, Harbin, Heilongjiang 150081, China*

► ***Original article***

Corresponding authors:
Wencheng Shao, Ph.D.,
Ziyin, Chen, Ph.D.
E-mail:
wenchengshao@outlook.com,
chenziyin1020@outlook.com

Received: April 2022
Final revised: October 2022
Accepted: November 2022

Int. J. Radiat. Res., April 2023; 21(2): 195-201

DOI: 10.52547/ijrr.21.2.3

Keywords: *Artificial intelligence cloud, auto-segmentation, early peripheral NSCLC, SBRT.*

[#]Xiaoping Lv is the co-first author.

ABSTRACT

***Background*:** The geometric and dosimetric accuracy of auto-segmentation OAR are of key importance for radiation oncologists who use auto-segmentation instead of manual segmentation. This study investigates the geometric and dosimetric accuracy of auto-segmentation OAR for early peripheral NSCLC using an artificial intelligence cloud online platform (AI Contour). ***Materials and Methods*:** AI Contour was used to perform the contour segmentation of OAR on twenty patients with early peripheral NSCLC, to evaluate geometric and dosimetric accuracies. Manual segmentation and auto-segmentation were performed to depict the outlines of the heart, lung, trachea, esophagus, and spinal cord. For geometric accuracy, the authors acquired and compared the Dice similarity coefficient, Jaccard coefficient, Hausdorf distance, Center of mass deviation, Inclusive index, and Sensitivity index. For dosimetric accuracy, the dose statistical differences between manual- and auto-segmentation were analyzed. The absolute irradiation volume deviation (AVD) and volume percentage deviation (VPD) for the V_5, V_{10}, V_{15}, and V_{20} of the lungs were assessed. The absolute irradiation dose deviation (ADD) and dose percentage deviation (DPD) for OAR were evaluated. ***Results*:** The DSC for each OAR was higher than 0.77. The dosimetric difference between manual and auto-segmentation was small and not significant (p>0.05). For the lung, the AVD was less than 7 mL, the VPD was less than 3%, the ADD of OAR was at most 0.4 Gy, and the DPD was less than 4%. ***Conclusion*:** The accuracy of the auto-segmented OAR for early peripheral NSCLC was acceptable based on AI Contour.

INTRODUCTION

Although computer techniques have been applied in radiotherapy, the segmentation of organs at risk (OAR) is still time-consuming and labor-intensive because radiotherapy practitioners need to manually contour the outlines of OAR and repeat the segmentation operations again and again for different patients. One of the main problems is that different radiation oncologists may have different understandings of OAR segmentation. This inevitably causes inter-observer variability during the segmentation of OAR and hinders the standardization of radiotherapy [1-5]. Existing studies have shown that lung cancer is a primary malignant tumor affecting the health of people worldwide because of high morbidity and mortality. The risk of lung cancer is related to age, smoking, environmental pollution, and many other factors [6-7]. With the advancement of the stereotactic body radiation therapy (SBRT) technology [8-10], many patients with early non-small cell lung cancer (NSCLC) have been treated with SBRT. The increase in the survival rate is making SBRT a viable option for an increasing number of NSCLC patients.

At present, there are numerous clinical procedures related to radiotherapy that occupy the working time of radiation oncologists, leaving them with less time to focus on the manual segmentation of OAR. Considering this difficulty, an accurate auto-segmentation technique that would assist radiotherapy physicians to complete the

[DOI: 10.52547/ijrr.21.2.3]

segmentation work accurately and efficiently would be very beneficial. Many studies have been conducted on developing auto-segmentation with deep learning technology for the delineation of targets in OAR [11-12]. However, the application of auto-segmentation software along with cloud technology has rarely been performed to treat early peripheral NSCLC patients. With the arrival of the 5G era and the current COVID-19 pandemic, telecommuting has become the new working mode and may become routine in the near future. In this study, artificial intelligence (AI) cloud technology was applied to perform the auto-segmentation of OAR for selected early peripheral NSCLC patients. By evaluating the geometric accuracy and dosimetric accuracy of auto-segmentation, it was found that applying AI could be a promising technology for the auto-segmentation of OAR. The purpose of this study is to enhance the uniformity and consistency of delineation of organs at risk in radiotherapy through artificial intelligence delineation technology, shorten delineation time, reduce the workload of radiotherapy physicians, and provide tools for radiation epidemiological research. The online artificial intelligence automatic delineation and the study of the dosimetry accuracy of the automatic delineation are the novelties of this study.

MATERIALS AND METHODS

Patient selection

Computed tomography (CT) images of twenty patients with early peripheral NSCLC treated with cyberknife SBRT from February 2018 to October 2021 were selected as research subjects. Eleven patients had squamous cell carcinoma, seven had adenocarcinoma, and two were diagnosed based on positron emission tomography-computed tomography (PET-CT). The criteria for inclusion and exclusion of patients were that they had early-stage peripheral non-small cell lung cancer, the tumor diameter was less than 5 cm, and all patients had completed SBRT treatment. Thirteen patients had right lung cancer, and seven patients had left lung cancer. There were sixteen males and four females, aged 49–80 years (median age 61.5 years), with tumor maximum diameter 1.64–4.72 cm (median diameter 3.44 cm), and tumor volume 2.97–24.95 cc (median volume 11.63 cc). The serial number of the institutional Ethical approval is 2022168 registered on October 21, 2022. Table 1 lists the main characteristics of the patients. Regarding the dose segmentation model, twelve patients were treated with 12 Gy × 5f (BED=132 Gy), and eight patients were treated with 10 Gy × 5f (BED=100 Gy). The limits of OAR were determined according to the corresponding literature requirements [13-14].

Table 1. Patients' characteristics.

Patient number	Age	Tumor location	Tumor diameter (cm)	PTV Volume (cc)	Dose segmentation model
1	52	RML	2.31	6.94	12 Gy × 5f
2	67	LLL	2.28	6.42	12 Gy × 5f
3	54	RUL	2.66	9.89	10 Gy × 5f
4	69	RLL	2.61	9.32	10 Gy × 5f
5	61	LLL	3.34	19.55	10 Gy × 5f
6	49	RML	1.90	3.59	12 Gy × 5f
7	51	RUL	1.93	3.79	12 Gy × 5f
8	72	RUL	2.54	8.56	12 Gy × 5f
9	59	RML	2.48	7.72	12 Gy × 5f
10	63	RUL	4.22	23.41	10 Gy × 5f
11	52	LUL	1.64	2.97	12 Gy × 5f
12	61	LUL	3.29	18.72	10 Gy × 5f
13	50	RLL	1.89	3.51	12 Gy × 5f
14	67	RUL	1.68	3.24	12 Gy × 5f
15	73	LUL	1.72	3.83	12 Gy × 5f
16	80	RML	2.77	10.53	10 Gy × 5f
17	55	RUL	2.45	7.73	12 Gy × 5f
18	53	LLL	3.79	22.59	10 Gy × 5f
19	64	LUL	2.32	6.54	12 Gy × 5f
20	78	LUL	4.72	24.95	10 Gy × 5f

Note: LUL: Left upper lobe; LLL: Left lower lobe; RUL: Right upper lobe; RML: Right middle lobe; RLL: Right lower lobe.

CT image acquisition and reference contours

In this study, CT image acquisition was carried out on a Siemens CT scanner (SOMATOM Definition AS). CT scanning parameters are: scanning voltage: 120 keV, current: 400 mA, Scanning layer thickness: 1 mm, Image size: 512×512, and the number of scanning layers ranges from 278 to 375 layers. Because Cyberknife image tracking has special requirements for scanning parameters, the scanning conditions are different from general radiotherapy. The CT images of twenty patients with a scanning layer thickness of 1 mm were uploaded to the LinkingMed artificial intelligence cloud outline platform (AI Contour, Version 3.1.6.0, LinkingMed Ltd., Beijing, China). The segmented structures included the heart, left and right lungs, trachea, esophagus, and spinal cord. On the AI Contour platform, manual segmentation was completed by a senior radiation oncology expert specializing in chest tumors and verified by another expert to ensure the accuracy of the segmentation. Manual segmentation was considered the standard.

Artificial intelligence cloud auto-segmentation

The Linking Med AI Contour was used to perform the auto-segmentation of OAR online. At present, most AI segmentation software are based on the U-net model [15], whereas AI Contour uses the 3D U-net model to perform the auto-segmentation of OAR. The 3D U-Net model is composed of two parts: down sampling and up sampling. Down sampling comprises seven dilated convolution layers and massive pooling layers. The up sampling comprises seven dilated convolution layers and three

[DOI: 10.52547/ijrr.21.2.3]

deconvolution layers. In addition to the inherent connection of down sampling and up sampling, a connection between two dilated adjacent convolutional layers was also added, and the extracted features were combined with increasing richness. A more detailed introduction to this method can be found in the literature [16]. At present, AI contours can achieve more than 100 OAR auto-segmentation tasks online. The specific working platform of the AI Contour is shown in figure 1 (AI Contour website: https:// aicontour.linkingmed.com/). AI Contour deploys servers and software on top of the cloud and distributes them to the users as needed. The AI Contour platform is a software-as-a-service (SAAS) technology [17], which eliminates the downloading and installation of user software and the storage of a large amount of patient data locally. Users can complete the segmentation remotely through a desktop, laptop, or even a tablet. The workflow of the AI contour consists of: (1) uploading the CT images to the cloud, (2) subsequent to upload, clicking on the patient that needs to be opened, and using the auto region of interest (ROI) function to auto-segment the OAR, (3) using the compare module to quantitatively compare the geometric accuracy of the auto-segmentation and manual-segmentation results.

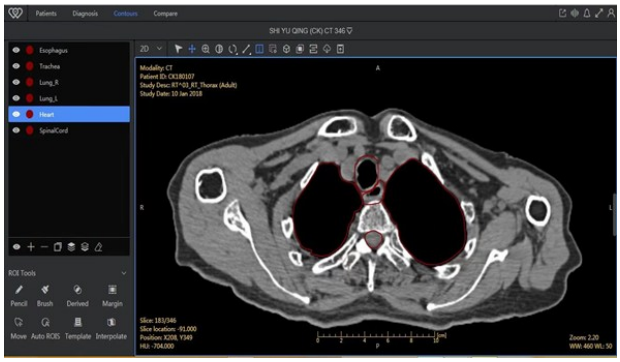

Figure 1. Illustration for the Web-based AI Contour working platform.

Geometric evaluation index of auto-segmentation and manual-segmentation

In this study, the geometric evaluation indicators include Dice similarity coefficient (DSC), Jaccard coefficient (JC), Hausdorff distance (HD), Center of mass deviation (CMD), Inclusive index (IncI), and Sensitivity index (SI). Those evaluation indicators can be respectively written as equations 1-6. In those equations, V_m is the volume of manual segmentation, V_a is the volume of auto-segmentation, X_m, Y_m, Z_m are the coordinates of the three coordinate axes of the manual delineation structure, X_a, Y_a, Z_a are the coordinates of the three coordinate axes of the automatically delineated structure. The meaning of the formula in the text is: (1) The DSC coefficient is used to evaluate the two delineation methods; (2) JC is the geometric similarity index of the delineated OAR; (3) HD is a measure of dissimilarity between two points sets; (4) CMD reflects the centroid distance of the two delineation methods; (5) IncI coefficient reflects the inclusion of V_a in V_m, that is, the probability that a voxel of V_a is actually a voxel of V_m; (6) SI reflects the matching probability of V_a and V_m.

1. Dice similarity coefficient (DSC) [18]

$$\mathrm{DSC} = \frac{2(Vm \cap Va)}{Vm + Va} \tag{1}$$

2. Jaccard coefficient (JC) [19]

$$\mathrm{JC} = \frac{Vm \cap Va}{Vm \cup Va} \tag{2}$$

3. Hausdorff distance (HD) [20]

The two sets X={x1,...,xn}, Y={y1,...,yn}, and the Hausdorff distance between these two sets of points is defined as

$$\mathrm{HD}(X,Y) = \max(h(X,Y), h(Y,X)) \tag{3}$$

Among them, $h(X,Y) = \max_{x \in X} \min_{y \in Y} \|x - y\|$

1. Center of mass deviation (CMD)

$$\mathrm{CMD} = \sqrt{(Xa - Xm)^2 + (Ya - Ym)^2 + (Za - Zm)^2} \tag{4}$$

2. Inclusive index (IncI) [21]

$$\mathrm{IncI} = \frac{Vm \cap Va}{Va} \tag{5}$$

3. Sensitivity index (SI) [22]

$$\mathrm{SI} = \frac{Vm \cap Va}{Vm} \tag{6}$$

Dosimetric evaluation index

The auto-segmentation structure, manual-segmentation structure, original CT image, and initially planned dose distribution are imported into the MIM software (6.9.4), whereby the evaluation workflow is used to extract dose volume histogram (DVH) data. For the left and right lung tissues, V_5, V_{10}, V_{15}, and V_{20} were obtained, and D_{max} was derived from the heart, trachea, esophagus, and spinal cord. Due to the slight differences in the total delineation volume of the left and right lung tissues between auto-segmentation and manual-segmentation, the irradiation volume of the lung tissue extracted in this study was the absolute volume. For the left and right lungs, $|\Delta V| = |V_{manual} - V_{auto}|$ and $|\Delta V_{\%}| = |(V_{manual} - V_{auto}) / V_{maual} * 100\%|$ in the quantitative analysis; for the heart, trachea, esophagus, and spinal cord, which are serial organs, $|\Delta D_{max}| = |D_{max\text{-}manual} - D_{max\text{-}auto}|$ and $|\Delta D_{max\%}| = |(D_{max\text{-}manual} - D_{max\text{-}auto}) / D_{max\text{-}manual} * 100\ \%|$

[DOI: 10.52547/ijrr.21.2.3]

for quantitative analysis.

Time comparison

The time for manual segmentation was set to the time elapsed from opening the CT images to the completion of the segmentation of the last OAR. The time for auto-segmentation was set to the time elapsed from uploading the CT images to the completion of the segmentation of the last OAR.

Statistical analysis

In this study, the data are represented by`X ± s, and the paired sample t-test was used for data that conformed to the normal distribution; the Wilcoxon signed-rank test was used for data that were not normally distributed. Statistical significance was set to $p < 0.05$. SPSS 22 software and the Shapiro-Wilk method were used for statistical analyses to check whether the data followed a normal distribution.

RESULTS

Geometric discrepancies

The specific AI contour auto-segmentation and manual-segmentation geometric accuracy index data are listed in table 2. Through comparisons, it was determined that the average value of DSC for each OAR was higher than 0.77, and the average value of JC was higher than 0.63. It was pointed out in the literature [23, 24] that when the DSC value is higher than 0.7, the auto-segmentation structure is acceptable. The DSC value of the left and right lungs were the highest (0.97 ± 0.01), and the esophagus DSC value was the lowest (0.77 ± 0.05), which may be the reason for the precise boundary of the lung tissue, the blurred boundary of the esophagus, and the small difference in contrast with the surrounding tissues. In terms of the parameters representing the two types of segmentation distances, the Lung-R had the largest HD with a value of (27.06 ± 13.88) mm, and the heart had the largest CMD with a value of (4.21 ± 2.97) mm. The mean value of the IncI of each OAR was higher than 0.70, and the mean value of SI was higher than 0.86. Based on the geometric accuracy data, the AI contour outline accuracy was acceptable. Figure 2 shows a case comparison chart of auto-segmentation and manual segmentation.

Dosimetric analysis

The dosimetric differences between the left and right lung tissues are compared in table 3. A comparative study suggested that the dosimetric difference was not significant in the left and right lung tissues ($p > 0.05$). In terms of absolute irradiation volume deviation |ΔV|, the maximum value was V_5 of Lung-R, ((6.51 ± 6.92) mL). In terms of volume percentage deviation |ΔV%|, the maximum value was also V_5 of Lung-R ((2.67 ± 1.87)%). This may be because V_5 was a low-dose area of irradiation, and the V_5 irradiation volume was markedly greater. For the other OAR, such as the heart, trachea, esophagus, and spinal cord, the specific data are shown in table 4. A comparative study suggested that the dosimetric difference was not significant in the heart, trachea, esophagus, and spinal cord ($p > 0.05$). In terms of the absolute dose deviation $|\Delta D_{max}|$, the maximum value was the trachea, with a value of (0.33 ± 0.36) Gy. In terms of dose percentage deviation $|\Delta D_{max\%}|$, the maximum value also was that of the trachea, with a value of (3.15 ± 2.61) %. From the differences in dosimetry data, it was observed that both the absolute and the percentage deviations were lower, indicating that the dosimetry similarity of the two types of segmentation was high. Figure 3 shows the specific dosimetric distribution for one patient.

Table 2. Geometric accuracy index data of auto-segmentation and manual segmentation (mean ±SD).

OAR	DSC	JC	HD (mm)	CMD (mm)	IncI	SI
Lung-L	0.97± 0.01	0.94± 0.03	22.53± 10.56	2.21± 1.42	0.97± 0.03	0.96± 0.03
Lung-R	0.97± 0.01	0.93± 0.02	27.06± 13.88	3.39± 3.90	0.97± 0.03	0.96± 0.03
Trachea	0.87± 0.03	0.77± 0.05	8.06± 2.94	1.99± 1.35	0.83± 0.09	0.90± 0.07
Esophagus	0.77± 0.05	0.63± 0.06	9.53± 5.09	2.70± 1.78	0.70± 0.09	0.86± 0.09
Spinal Cord	0.88± 0.03	0.78± 0.05	4.84± 1.73	1.47± 0.82	0.87± 0.07	0.89± 0.07
Heart	0.91± 0.01	0.84± 0.02	15.71± 8.10	4.21± 2.97	0.91± 0.06	0.90± 0.05

DSC is the Dice similarity coefficient, JC is the Jaccard coefficient, HD is the Hausdorff distance, CMD is the center of mass deviation, IncI is the inclusive index, and SI is the sensitivity index.

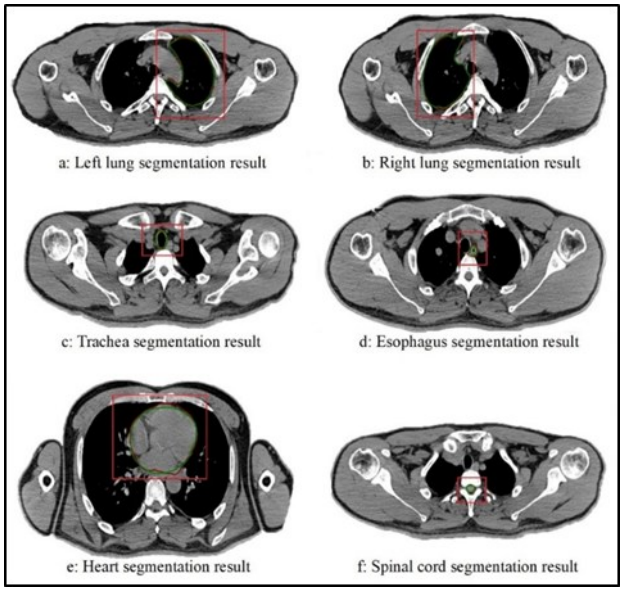

Figure 2. In a case comparison chart of auto- and manual-segmentation, the results of auto-segmentation are in red, and the results of manual-segmentation are in green. Regions of interest were depicted with red lines.

[DOI: 10.52547/ijrr.21.2.3]

Table 3. Lung tissue dosimetric data of two kinds of segmentation (Mean ± SD).

OAR	Item	Manual (ml)	Auto (ml)	*t/Z*	*P*	|ΔV| (ml)	|ΔV%|
Lung-L	V_5	141.96±203.75	144.04±208.46	-1.349	0.177[b]	4.55±6.51	2.93±2.31
	V_{10}	60.93±99.85	61.26±100.63	-0.676	0.499[b]	1.34±2.49	1.03±1.92
	V_{15}	34.59±57.37	34.76±57.67	-0.507	0.612[b]	0.77±1.49	0.85±1.46
	V_{20}	22.38±37.49	22.49±37.63	-0.338	0.735[b]	0.61±1.19	0.94±1.56
Lung-R	V_5	224.71±186.85	227.13±188.08	-1.165	0.258[a]	6.51±6.92	2.67±1.87
	V_{10}	105.16±98.66	105.56±97.75	-0.781	0.435[b]	2.80±3.24	2.55±2.34
	V_{15}	60.15±63.59	60.38±62.99	-0.534	0.594[b]	1.56±2.14	1.93±2.19
	V_{20}	40.36±44.73	40.51±44.32	-0.524	0.600[b]	1.01±1.46	1.75±2.30

a: Paired sample t-test; b:Wilcoxon signed-rank test. $|\Delta V|=|V_{manual}-V_{auto}|$, $|\Delta V\%| = |(V_{manual}-V_{auto})/V_{manual}*100\%|$

Table 4. Dosimetric data of the heart, trachea, esophagus, and spinal cord of two types of segmentation (mean ±SD).

OAR	Item	Manual (Gy)	Auto(Gy)	*t/Z*	*P*	$\|\Delta D_{max}\|$(Gy)	$\|\Delta D_{max\%}\|$	Max$\|\Delta D_{max}\|$(Gy)	Min$\|\Delta D_{max}\|$(Gy)
Trachea	D_{max}	9.30±5.78	9.37±6.04	-0.348	0.727[b]	0.33±0.36	3.15±2.61	1.24	0.02
Esophagus	D_{max}	7.31±3.37	7.24±3.41	1.459	0.161[a]	0.15±0.16	2.36±2.12	0.56	0.03
Spinal Cord	D_{max}	6.12±2.59	6.08±2.60	2.003	0.060[a]	0.08±0.08	1.57±1.74	0.27	0.01
Heart	D_{max}	10.86±6.25	11.05±6.45	-1.857	0.079[a]	0.31±0.37	2.60±2.30	1.19	0.01

a: Paired sample t-test; b:Wilcoxon signed-rank test. $|\Delta V|=|V_{manual}-V_{auto}|$, $|\Delta V\%| = |(V_{manual}-V_{auto})/V_{manual}*100\%|$

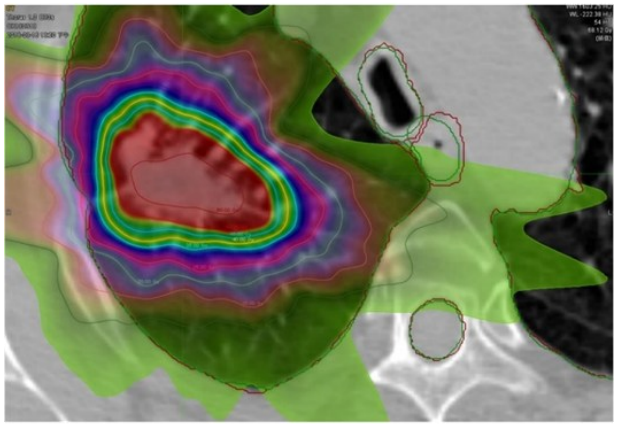

Figure 3. The specific dosimetric distribution of a selected patient. (Dose segmentation is 10 Gy × 5f). The results of auto-segmentation are in red, and the results of manual-segmentation are in green.

Time analysis

The auto-segmentation time was (270.70±28.25) s, in contrast to the manual-segmentation time of (2463.10±158.10) s. There was a significant difference in the segmentation times (p<0.001) indicating that the auto-segmentation method saved significantly more time.

DISCUSSION

In the current study, the AI Contour cloud platform was used to conduct OAR auto-segmentation based on artificial intelligence on early peripheral NSCLC cases. It was found that the DSC value of each OAR was higher than 0.77; the JC value was higher than 0.63; and the geometric accuracy was acceptable. Cloud segmentation technology has the potential to avoid gathering as many subjects as possible. More importantly, the web-based segmentation mode improves work efficiency. Currently, research on auto-segmentation has been mainly based on the atlas and two types of deep learning technologies. Many previous atlas-based auto-segmentation studies have mainly focused on head and neck tumors and prostate cancer [25-26]. Auto-segmentation of the atlas often provides unsatisfactory results for smaller sized organs with inconspicuous contrast changes. Artificial intelligence technology based on deep learning is expected to solve this problem. An auto-segmentation model based on deep learning technology learns high-quality manual segmentation samples. When a new set of images is input, the auto-segmentation is carried out based on the well-trained model. Recently, many comparative studies on deep learning technology and atlas technology have been conducted [27-28]. These research results have shown that the segmentation quality of deep learning technology is generally higher than that of atlas technology. The auto-segmentation software based on deep learning saves the user from building a database as it can be directly used. In addition, using auto-segmentation software more frequently is conducive to the transition of radiotherapy from manual-segmentation to auto-segmentation mode.

The results of this study suggested that the final dosimetric accuracy of the auto-segmentation was not only correlated with geometric simplicity, but also correlated with tumor-OAR geometric relationship, irradiation technique, dose distribution, etc. Our results are similar to those of Robert *et al.* [29] for the auto-segmentation of breast cancer. However, more attention should be paid when the spinal cord and brain stem are around an area with a high dose gradient, even when high geometric accuracy is achieved by auto-segmentation. For geometric deviations precisely in the high-dose gradient area, the dosimetric deviations are more significant [30]. With the advancement of radiotherapy technology and the upgrade of equipment, patients with early peripheral NSCLC may have an increasingly longer survival rate after SBRT treatment. For patients with a long survival period after SBRT, the AI contour auto-segmentation function can also be used to conduct many retrospective studies to validate radiation

[DOI: 10.52547/ijrr.21.2.3]

injury models (normal tissue complication probability, NTCP). The results of this study are mainly related to early peripheral NSCLC. Early central lung tumors and other chest tumors are more complicated to investigate. Thus, further research into tumors surrounded by more complex anatomies still needs to be performed in the future.

Our results demonstrate the feasibility of applying cloud delineation technology for this disease type. With the advent of the 5G era, radiotherapy is expected to rely more heavily on cloud technology. Cloud technology and cloud services are Internet-based computing models, which can be configured dynamically as required because of the distributed computing technology aspect. The computing processing program is divided into relatively small systems throughout the network, and multiple servers perform tasks in parallel. After analysis and processing, the results are summarized and sent back to the user. The advantages of cloud technology in the field of radiation therapy are manifold: (1) Cloud technology can be realized in a mobile office enabling remote segmentation, remote planning, and remote collaboration, optimizing the time of radiotherapy practitioners, saving time and space, and improving work efficiency; (2) users do not need to download and install the segmentation software if they can perform segmentation work by logging into the website; (3) users do not need to store a large number of images and other data locally because all data can be stored in the cloud and can be downloaded when needed, thereby reducing the operation and maintenance costs of the radiotherapy unit; (4) relatively small radiotherapy units can rely on smart products in the cloud to standardize treatment and narrow the gap between different units. The markedly increased efficiency of cloud technology may change the preferred analysis working model.

CONCLUSION

The results of this study suggest that the AI Contour cloud technology-based intelligent segmentation platform can efficiently perform auto-segmentation of OAR for early peripheral NSCLC and is acceptable in terms of both geometric and dosimetric accuracy. However, it should be noted that applying auto-segmentation in the clinical setting requires review and approval by an experienced radiation oncology team. In the era of precision therapy, radiotherapy of lung cancer also requires the auto-segmentation of more structures such as the chest wall, bronchus, large blood vessels, and even brachial plexus nerves.

ACKNOWLEDGMENTS

We would like to thank LinkingMed Company for its technical support during auto-segmentation of OARs.

***Conflicts of Interest*:** The authors declare no conflict of interest.

***Ethical consideration*:** The study was conducted in accordance with the principles of the Declaration of Helsinki. All diagnostic and therapeutic procedures were performed according to the current standard-of-care and after receiving the patients' informed consent. No diagnostic or therapeutic acts were performed for the purpose of research. This is only a retrospectives study based on radiotherapy dose data, thus patient consent for inclusion was waived.

***Author contribution*:** Ziyin Chen analyzed the DVH data and contributed in writing the manuscript; Xiaoping Lv analyzed the DVH data; Chunyan Bai and Lili Xu contributed in manually segmenting the OARs; Wencheng Shao contributed in writing and revising the manuscript.

REFERENCES

1. Dewas S, Bibault JE, Blanchard P, Vautravers DC, *et al.* (2011) Delineation in thoracic oncology: a prospective study of the effect of training on contour variability and dosimetric consequences. *Radiat Oncol, **6**(1): 1-9*.
2. Altorjai G, Fotina I, Lütgendorf CC, Stock M, *et al.* (2012) Cone-beam CT-based delineation of stereotactic lung targets: the influence of image modality and target size on interobserver variability. *Int J Radiat Oncol Biol Phys*, **82**(2): 265-272*.
3. Persson GF, Nygaard DE, Hollensen C, *et al*. (2012) Interobserver delineation variation in lung tumor stereotactic body radiotherapy. *Br J Radiol, **85**(1017): 654-660.*
4. Vinod SK, Jameson MG, Min M, Holloway LC (2016) Uncertainties in volume delineation in radiation oncology: A systematic review and recommendations for future studies. *Radiother Oncol, **121**(2): 169-179.*
5. Wee CW, An HJ, Kang HC, Kim HJ, Wu HG (2018) Variability of gross tumor volume delineation for stereotactic body radiotherapy of the lung with Tri-60Co magnetic resonance image-guided radiotherapy system (ViewRay): A comparative study with magnetic resonance- and computed tomography-based target delineation. *Technol Cancer Res Treat, **17**: 1-7.*
6. Bray F, Ferlay J, Soerjomataram I, Siegel RL, *et al.* (2018) Global cancer statistics 2018: GLOBOCAN estimates of incidence and mortality worldwide for 36 cancers in 185 countries. *CA Cancer J Clin, **68**(6): 394-424.*
7. Chen W, Zheng R, Baade PD, Zhang S, *et al.* (2016) Cancer statistics in China, 2015. *CA Cancer J Clin, **66**(2): 115-132.*
8. Chang JY, Senan S, Paul MA, *et al.* (2015) Stereotactic ablative radiotherapy versus lobectomy for operable stage I non-small-cell lung cancer: a pooled analysis of two randomized trials. *Lancet Oncol, **16**(6): 630-637.*
9. Shinde A, Li R, Kim J, Salgia R, Hurria A, Amini A (2018) Stereotactic body radiation therapy (SBRT) for early-stage lung cancer in the elderly. *Semin Oncol, **45**(4): 210-219*.
10. Prezzano KM, Ma SJ, Hermann GM, Rivers CI, *et al.* (2019) Stereotactic body radiation therapy for non-small cell lung cancer: A review. *World J Clin Oncol, **10**(1): 14-27.*
11. Wang C, Tyagi N, Rimner A, Hu Y, *et al.* (2019) Segmenting lung tumors on longitudinal imaging studies via a patient-specific adaptive convolutional neural network. *Radiother Oncol, **131**: 101-107.*
12. Song Y, Hu J, Wu Q, Xu F, Nie S, *et al.* (2020) Automatic delineation of the clinical target volume and organs at risk by deep learning for rectal cancer postoperative radiotherapy. *Radiother Oncol, **145**: 186-192.*
13. Benedict SH, Yenice KM, Followill D, *et al.* (2010) Stereotactic body radiation therapy: The report of AAPM Task Group101. *Med Phys, **37**(8): 4078-4101.*
14. Hanna GG, Murray L, Patel R, *et al.* (2018) UK consensus on normal tissue dose constraints for stereotactic radiotherapy. *Clin Oncol, **30**(1): 5-14.*

[DOI: 10.52547/ijrr.21.2.3]

15. Zunair H and Hamza AB (2021) Sharp U-Net: depthwise convolutional network for biomedical image segmentation. *Comput Biol Med,* ***136****: 1-13.*
16. Sun Y, Shi H, Zhang S, Wang P, *et al.* (2019) Accurate and rapid CT image segmentation of the eyes and surrounding organs for precise radiotherapy. *Med Phys,* ***46****(5): 2214-2222.*
17. Sharma A and Kaur P (2021) TOSDS: Tenant-centric Object-based Software Defined Storage for Multitenant SaaS Applications. *Arab J Sci Eng,* ***46****(9): 9221-9235.*
18. Dice LR (1945) Measures of the amount of ecologic association between species. *Ecology,* ***26****(3): 297-302.*
19. Jaccard P (1912) The distribution of the flora in the alpine zone. *New Phytol,* ***11****(2): 37-50.*
20. Taha AA and Hanbury A (2015) An efficient algorithm for calculating the exact Hausdorff distance. *IEEE Trans Pattern Anal Mach Intell,* ***37****(11): 2153-2163.*
21. Macchia ML, Fellin F, Amichetti M, Cianchetti M, *et al.* (2012) Systematic evaluation of three different commercial software solutions for automatic segmentation for adaptive therapy in head -and-neck, prostate, and pleural cancer. *Radiat Oncol,* ***7****(1):1-16.*
22. Tsuji SY, Hwang A, Weinberg V, Yom SS, *et al.* (2010) Dosimetric evaluation of automatic segmentation for adaptive IMRT for head-and-neck cancer. *Int J Radiat Oncol Biol Phys,* ***77****(3): 707-714.*
23. Zijdenbos AP, Dawant BM, Margolin RA, Palmer AC (1994) Morphometric analysis of white matter lesions in MR images: method and validation. *IEEE Trans Med Imaging,* ***13****(4): 716-724.*
24. Artaechevarria X, Munoz-Barrutia A, Ortiz-de-Solorzano C (2009) Combination strategies in multi-atlas image segmentation: application to brain MR data. *IEEE Trans Med Imaging,* ***28****(8): 1266 -1277.*
25. Daisne JF and Blumhofer A (2013) Atlas-based automatic segmentation of head and neck organs at risk and nodal target volumes: a clinical validation. *Radiat Oncol,* ***8*** *(1):1-11.*
26. Sjöberg C, Lundmark M, Granberg C, Johansson S, *et al.* (2013) Clinical evaluation of multi-atlas based segmentation of lymph node regions in head and neck and prostate cancer patients. *Radiat Oncol,* ***8****(1): 224-229.*
27. Lustberg T, van Soest J, Gooding M, *et al.* (2018) Clinical evaluation of atlas and deep learning-based automatic contouring for lung cancer. *Radiother Oncol,* ***126****(2): 312-317.*
28. Dijk V, Lisanne V, Bosch VD, *et al.* (2020) Improving automatic delineation for head and neck organs at risk by Deep Learning Contouring. *Radiother Oncol,* ***142****: 115-123.*
29. Kaderka R, Gillespie EF, Mundt RC, *et al.* (2019) Geometric and dosimetric evaluation of atlas based auto-segmentation of cardiac structures in breast cancer patients. *Radiother Oncol,* ***131****: 215-220.*
30. Fung N, Hung WM, Sze CK, *et al.* (2020) Automatic segmentation for adaptive planning in nasopharyngeal carcinoma IMRT: Time, geometrical, and dosimetric analysis. *Med Dos,* ***45****(1): 60-65.*

[DOI: 10.52547/ijrr.21.2.3]